THE AMERICAN SOCIETY OF MECHANICAL ENGINEERS
345 E. 47th St., New York, N.Y. 10017

94-GT-457

THE DEVELOPMENT OF THE MEAN FLOW AND TURBULENCE STRUCTURE IN AN ANNULAR S-SHAPED DUCT

K. M. Britchford, J. F. Carrotte, S. J. Stevens, and J. J. McGuirk
Department of Transport Technology
University of Technology
Loughborough, Leicestershire, United Kingdom

ABSTRACT

This paper describes an investigation of the mean and fluctuating flow field within an annular S-shaped duct which is representative of that used to connect the compressor spools of aircraft gas turbine engines. Data was obtained from a fully annular test facility using a 3-component Laser Doppler Anemometry (LDA) system. The measurements indicate that development of the flow within the duct is complex and significantly influenced by the combined effects of streamwise pressure gradients and flow curvature. In addition CFD predictions of the flow, using both the k-ε and Reynolds stress transport equation turbulence models, are compared with the experimental data. Whereas curvature effects are not described properly by the k-ε model, such effects are captured more accurately by the Reynolds stress model leading to a better prediction of the Reynolds shear stress distribution. This, in turn, leads to a more accurate prediction of the mean velocity profiles, as reflected by the boundary layer shape parameters, particularly in the critical regions of the duct where flow separation is most likely to occur.

NOMENCLATURE

A	area
C_p	pressure coefficient
C_f	wall friction coefficient (= $(U_\tau/U_{mean})^2$)
K_{eff}	effective curvature of flow at mid-passage
H	boundary layer shape parameter (= δ*/θ)
L	S-shaped duct axial length
P, p	total pressure, static pressure
R	radius of flow curvature
U	mean streamwise velocity component
U_c	streamwise velocity at mid-passage
U_p	potential velocity
U_τ	friction velocity (= $(\tau_w/\rho)^{1/2}$)
h	passage height
k	turbulent kinetic energy (= $\frac{1}{2}(\overline{u^2}+\overline{v^2}+\overline{w^2})$)
r	radius
u	fluctuating streamwise velocity component
$\overline{uv}$	Reynolds shear stress component
x	axial distance
y_c	distance from mid passage
y	distance from casing surface along the traverse plane
δ	boundary layer thickness
δ*	boundary layer displacement thickness (= $\int (1-U/U_p)\,dy$)
θ	boundary layer momentum thickness (= $\int (U/U_p)(1-U/U_p)\,dy$)
ε	dissipation rate of turbulent kinetic energy
μ, ν	molecular viscosity, kinematic viscosity (= μ/ρ)
ρ	density
τ_w	wall shear stress (= $\mu\partial U/\partial y$)

Subscripts

i	inner casing
o	outer casing
in	S-shaped duct inlet (x/L=0.0)
ex	S-shaped duct exit (x/L=1.0)
mean	area weighted spatial average

Superscripts

‾	time average
~	mass weighted spatial average

INTRODUCTION

In order to optimise the performance of multi-spool compressors found within aircraft gas turbine engines, the diameter of each spool must reduce as air density increases through the compression system. Thus, the annular

Presented at the International Gas Turbine and Aeroengine Congress and Exposition
The Hegue, Netherlands – June 13–16, 1994

interconnecting duct between the spools takes on the form of an 'S' shape. In addition, for aircraft applications this change of diameter must be achieved in the shortest possible length, so as to minimise engine weight, whilst avoiding flow separation since this would adversely affect the performance of the downstream compressor. However, these objectives are difficult to achieve because of the complex nature of the flow which develops under the combined influence of pressure gradient and curvature. In addition, the situation is further complicated by the presence of struts, which carry loads or services, and the influence of inlet conditions arising from the upstream compressor.

As the flow follows a curved path within the S-shaped duct a modification of the static pressure field occurs. Within the first bend a positive radial pressure gradient is therefore present, with the pressure close to the outer casing being higher than that adjacent to the inner. However, this situation is reversed within the second bend as the flow is returned to the axial direction. Consequently streamwise pressure gradients arise which influence the boundary layer development along each casing surface. In addition, the turbulence within these boundary layers is directly affected by the streamline curvature. For example, the imbalance that exists between the centripetal acceleration of a turbulent fluid element and its surrounding pressure field gives rise to a stabilising influence over a convex surface, thereby reducing turbulent mixing. In contrast, over a concave surface the effect is destabilising which gives rise to increased turbulent mixing. Naturally these effects can have a significant impact on the development of the casing wall boundary layers. Furthermore, although a large number of studies have been made on these topics, the majority of investigations have considered the effects in isolation only.

An early study of the effects that streamwise pressure gradients have on a turbulent boundary layer was undertaken by Schubauer and Klebanoff (1951). Upon encountering a pressure gradient it was noted that a change in the boundary layer's mean velocity profile occurs. In particular, the pressure gradient will have a larger effect on the momentum of the slower moving fluid, adjacent to the surface, compared with the higher velocity flow in the outer regions of the boundary layer. Furthermore, since the production of turbulence is a function of velocity gradient, these profile changes must also lead to a modification of the Reynolds stresses and their distribution within the boundary layer. Thus, upon encountering a positive pressure gradient the boundary layer in close proximity to the surface decelerates. As shown by Schubauer and Klebanoff (1951) this results in a reduction of the wall shear stress whilst the Reynolds shear stress increases, with the location of the maximum value moving away from the wall. It is this gradient of shear stress between the surface and the maximum value location that leads to a 'diffusion' of momentum towards the wall, and allows the near-wall fluid to advance against the increasing pressure. Alternatively, when a favourable pressure gradient is applied the relative increase in momentum at the surface increases the wall shear stress, but the level of Reynolds shear stress across the remainder of the boundary layer tends to reduce. It should also be noted that, within an annular S-shaped duct, the magnitude and sign of the streamwise pressure gradient continually varies. The effect of such an alternating gradient on a flat wall turbulent boundary layer was investigated by Tsuji and Morikawa (1976). Their measurements of mean velocity and Reynolds shear stress showed that such a boundary layer increasingly departs from equilibrium. This is because the mean velocity profile responds rapidly to the applied pressure gradient, but a greater period of time is required for the turbulence to respond.

The effects of streamline curvature have been studied by a large number of authors, with Bradshaw (1973) providing a substantial review of the early work. This indicated that even for mild curvature ($\delta/R \approx 0.01$) a significant effect on turbulence was observed. However, whereas the effects of an applied pressure gradient is first apparent adjacent to the wall, the streamline curvature effects are initially observed within the outer regions of the boundary layer. This was first observed by So and Mellor (1972) and later confirmed by Gillis and Johnston (1983) and Barlow and Johnston (1988) whose results, with strong curvature present ($\delta/R \approx 0.1$), show that for convex curvature the Reynolds shear stress reduces to zero in the outer part of the layer but almost doubles for the concave case. However, the inner layer was relatively unaffected by curvature with the law of the wall still applicable in this region. For mild curvature, Meroney and Bradshaw (1975) and Shivaprasad and Ramaprian (1978) still observed significant changes to the turbulence structure and the differing effects of convex and concave curvature are explained in detail by Muck et al. (1985) and Hoffmann et al. (1985). Mild convex curvature will attenuate the pre-existing turbulence whereas concave curvature leads to a significant change of the turbulence structure, induced directly by the curvature and indirectly by the formation of longitudinal vortices. If these vortices are fixed in space by some upstream disturbance then spanwise variations in time averaged flow properties are observed. However, if the flow is relatively free of such disturbances then Barlow and Johnston (1988) have shown that destabilising curvature leads to the formation of large scale structures with no fixed spatial location.

Within an annular S-shaped duct the pressure gradient and curvature vary continuously along the duct. Although these effects have been mostly studied in isolation, one example where such effects are simultaneously present is described by Baskaran et al. (1987) concerning the flow over a curved hill. It was noted that at the transition from concave to convex curvature, in a region of strong favourable pressure gradient, an 'internal layer' was formed whose behaviour was identical to that of a newly formed turbulent boundary layer. In this layer the effects of the pressure gradient were predominant and curvature effects relatively small, although in the flow above this layer curvature effects dominated. Combined pressure gradient and curvature effects were also studied by Bandyopadhyay and Ahmed (1993) for an S-shaped rectangular duct. Unfortunately their flow is dominated by secondary end wall effects but they also confirm the formation of an internal layer at the point of curvature transition.

In contrast to these experimental studies curvature effects have been investigated by Moser and Moin (1987) using Direct

Numerical Simulation (DNS). Their results indicated that the magnitude of the terms in the shear stress transport equations are significantly modified by curvature and that using gradient diffusion models for the higher order terms is inappropriate. In addition, Jones and Manners (1989) performed CFD calculations on a curved annular diffuser, incorporating both concave and convex curvature, for which comprehensive mean velocity and shear stress measurements were obtained by Stevens and Eccleston (1969). They showed that the Reynolds stress transport equation model, in contrast to the k-e model, was able to predict most of the streamline curvature effects. However, the use of various modelling assumptions still limited the accuracy of this prediction.

The objective of this investigation was to obtain comprehensive measurements of the mean flow and turbulence structure within an annular S-shaped duct and use the data as a test case for CFD methods. The duct geometry is typical of that which may be found within a gas turbine engine and Britchford et al. (1993) have already shown how compressor generated inlet conditions reduce the tendency for the flow to separate along the inner casing of this duct. However, in the current paper only axi-symmetric inlet conditions, developed in an upstream entry length, are considered. The development of the flow is described as it is subjected to the varying pressure gradients and duct curvatures. In addition, measurements of the mean velocity and Reynolds shear stress are also compared with the CFD calculations previously described by Britchford et al. (1993).

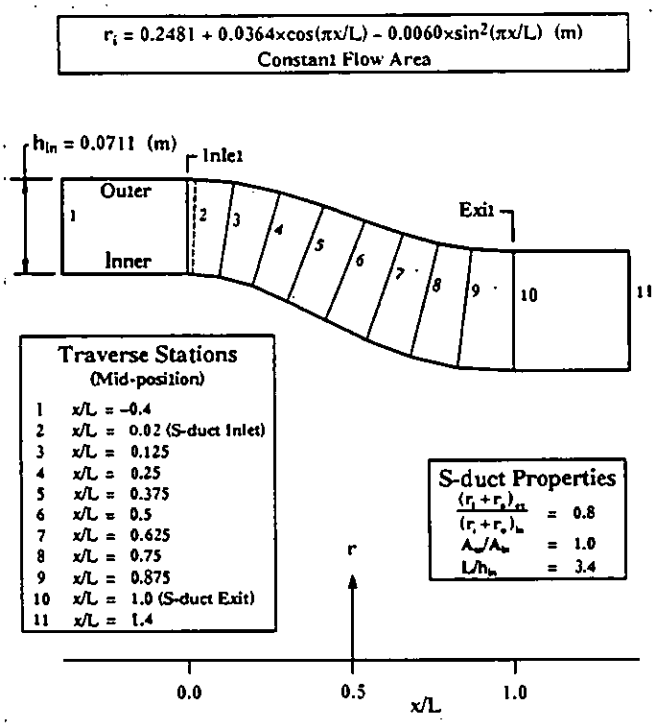

FIGURE 1 S-SHAPED DUCT GEOMETRY AND MEASUREMENT TRAVERSE PLANES

EXPERIMENTAL FACILITY

A detailed description of the experimental facility is given by Britchford et al. (1993). Air is drawn from atmosphere into a large plenum prior to passing through an entry flare which also contains a honeycomb flow straightener. After a contraction the flow adjacent to the inner and outer casings is artificially tripped before entering an inlet section 7 hydraulic diameters long. An axial compressor stage can then be incorporated immediately upstream of the S-shaped duct in order to generate engine representative inlet conditions. Alternatively, the compressor can be removed to provide a 'clean' configuration with the entry conditions to the S-shaped duct being determined by boundary layer development along the inlet length. The duct itself (Fig. 1) is of constant flow area with an inlet passage height (h_{in}) of 71.1 mm, an axial length (L/h_{in}) of 3.4 and an exit to inlet mean radius ratio of 0.8. Along the mean line the radius of curvature at inlet is $2.55h_{in}$ and at outlet is $3.23h_{in}$. This combination of axial length and reduction in mean duct radius were chosen to produce wall pressure gradients typical of existing engine design practice. Downstream of the duct a parallel settling length of 3.1 hydraulic diameters is provided prior to the air passing into the exhaust plenum and being expelled to atmosphere. With the axial compressor removed, air is drawn through the facility by 2 centrifugal compressors located within the exhaust system. All the results presented were obtained at a Reynolds number, based on inlet hydraulic diameter and mean passage velocity, of 2.8×10^5. Measurements were made at 11 streamwise stations (Fig. 1) and, since the flow has been shown to be axi-symmetric, were performed by traversing across the passage at a fixed circumferential location.

INSTRUMENTATION

As described in detail by Carrotte et al. (1993), all measurements were obtained using a DANTEC 3-channel fibre optic LDA system. The 3 channels were colour separated with each channel incorporating a 40 MHz frequency shift to eliminate fringe bias. Optical access to the duct was obtained through several Plexiglas windows of 1 mm thickness, the curvature of each window corresponding to that of the duct so as to avoid influencing boundary layer development. Seeding was provided by a TSI six jet atomiser using a relatively low viscosity oil. The resulting particles of approximately 0.5 μm diameter were injected using a single radial pipe, with multiple outlet holes, located in the plenum above the measurement position. Signals received from each channel, due to the passage of particles through the measurement volume, were processed in the frequency domain using 57N10 Burst Spectrum Analysers (BSAs).

Spatial measurement resolution within the duct is determined by the transmitting and receiving optics of the LDA system. Each channel had a beam separation at the lens of 16 mm with a focal length of 120 mm which gave a control volume size of

approximately 0.1x0.1x1.5 mm. However, an effective measurement volume of 0.1x0.1x0.3 mm was achieved through off-axis detection with an included angle of approximately 40° between each channels transmitting and receiving optics. Within the S-shaped duct the position of this measurement volume, relative to each casing surface, could be determined to within 60 μm (Carrotte et al., 1993). To ensure coincidence of the 3 control volumes all 6 laser beams were aligned to pass simultaneously through a pin hole of 50 μm diameter. In addition, the pin hole was also used to track the path of each beam which allowed beam alignment, relative to the traverse direction, to be determined to within ±0.2°.

All measurements were performed with coincidence filtering i.e. data were only recorded when bursts were simultaneously registered and validated by all 3 BSAs. A nominal 10,000 bursts were collected at each data point but the internal validation process and coincidence filtering meant that the number of actual coincidence bursts analysed was significantly less. Thus, within the central region of the passage 5000 samples or more were validated at each location. However, towards each casing the signal to noise ratio (SNR) reduces so that 2000 bursts or less were validated at locations within 1 mm of each casing surface. At less than 0.4 mm from a surface no meaningful data could be obtained due to the poor SNR. The limited optical access resulted in the measured velocity components (U_{BSA1}, U_{BSA2}, U_{BSA3}) being non-orthogonal. As described by Carrotte et al. (1993) a transformation matrix was therefore applied during processing in order to convert the data into 3 mutually orthogonal components aligned with the traverse plane. These were the streamwise component normal to the traverse plane (U), the cross-passage component (V) and circumferential component (W).

DATA REDUCTION AND EXPERIMENTAL ERRORS

As the flow passes through the duct, the potential core of the velocity profile behaves as a free vortex, with the streamwise velocity decreasing with increasing distance from the centre of curvature. This behaviour is used to estimate the effective curvature of the flow (K_{eff}), along the centreline of the duct, which differs from the duct's geometrical curvature due to the displacement thickness associated with each casing boundary layer. During this process the mid-passage (y_c=0) velocity (U_c) along with K_{eff} is determined to give the best (least square) fit of a free vortex potential velocity distribution ($U_p = U_c/(1+K_{eff}\, y_c)$ to the data in the core region. Having established this distribution for each traverse station, the boundary layer properties (δ, δ^*, θ) were calculated with respect to this potential velocity distribution. The wall shear stress (τ_w) was estimated by calculating the friction velocity (U_τ) at each position (y) within the boundary layer in order for the measured streamwise velocity (U) to fit the law of the wall ($U/U_\tau = 2.44 \ln(U_\tau y/v) + 4.88$). This produces a distribution of U_τ which tends towards a constant value at small distances from the casing surface where the law of the wall is applicable.

A detailed analysis of the magnitude and sources of experimental errors, for measurements similar to those described in this paper, is outlined by Carrotte et al. (1993). It was estimated that over the majority of the annulus, mean velocities could be obtained within ±0.1 m/s of their true values. However due to the poor SNR this error increased to ±2% of the local streamwise velocity within 0.9 mm of each casing surface. Similarly, it was thought that within the central passage region Reynolds stresses were within ±5% of their true values, with the uncertainty increasing to ±8% when 0.9 mm or less from each casing. At the majority of positions a reasonable estimate (±5%) of the wall shear stress (τ_w) could be obtained from the mean velocity profile and log law using the technique previously outlined. However, downstream of a concave surface the indicated friction velocity (U_τ) continued to rise towards the casing surface. Hence, in such regions very few of the experimental data points close to the surface fall within the log law region and so the wall value (τ_w) can only be broadly estimated (±10%). However, overall it should be noted there is good agreement between the wall shear stress values derived from the mean velocity data and those indicated by extrapolation of the measured shear stress distribution.

In general, a greater amount of experimental scatter was observed within the outer casing boundary layer measurements, compared with those of the inner, despite a relatively large number of samples being collected in this region. As suggested by Barlow and Johnston (1988) this may indicate the presence of large scale structures due to the concave curvature within the first bend. The relatively long time scales associated with these features would increase the amount of scatter in these measurements.

THEORETICAL METHODS ADOPTED

The time-averaged flow through the annular S-shaped duct has been predicted using the CFD approach of Jones and Manners (1989). The predictions are described in more detail by Britchford et al. (1993). The turbulence models used in the calculation are the standard k-ε and Reynolds stress closures. The computational procedure used to solve the mean flow and turbulence model equations is based on a transformation to a boundary conforming orthogonal co-ordinate system. Grid orientated velocities and Reynolds stresses are adopted which allows a staggered mesh approach to be used to avoid pressure/velocity and stress/strain rate decoupling. In order to avoid the need to code a large number of extra terms in the transformed equations, an isotropic gradient diffusion model is adopted for the triple velocity correlations. A pressure correction algorithm is used to obtain the pressure field and standard equilibrium wall functions were employed at solid boundaries. The streamline orientated mesh produced grid independent solutions with 80 cross-stream by 100 streamwise cells; selected streamwise locations were aligned with the experimental traverse planes to enable direct comparison.

TABLE 1 BOUNDARY LAYER PROPERTIES

x/L	Stn. No.	Inner Wall δ (mm)	δ* (mm)	θ (mm)	H	C_f (x10^3)	Outer Wall δ (mm)	δ* (mm)	θ (mm)	H	C_f (x10^3)
-0.400	1	17.0	2.40	1.80	1.33	1.92	17.0	2.40	1.80	1.33	2.05
0.020	2	15.5	1.70	1.35	1.26	2.88	20.5	3.50	2.45	1.43	1.30
0.125	3	15.0	1.65	1.30	1.27	3.12	20.5	3.70	2.65	1.40	1.20
0.250	4	16.0	1.95	1.50	1.30	2.59	20.0	3.35	2.50	1.34	1.51
0.375	5	18.0	3.05	2.15	1.42	1.30	19.5	2.75	2.15	1.28	2.31
0.500	6	21.0	4.35	2.80	1.55	0.84	20.0	2.30	1.85	1.24	3.04
0.625	7	24.5	6.00	3.65	1.64	0.58	21.0	2.20	1.80	1.22	3.61
0.750	8	28.5	7.30	4.40	1.66	0.51	22.0	2.25	1.85	1.22	3.52
0.875	9	30.0	7.50	4.65	1.61	0.65	23.0	2.50	2.00	1.25	2.88
1.000	10	29.0	5.80	4.05	1.43	1.20	24.5	3.00	2.35	1.28	2.18
1.400	11	27.5	4.65	3.50	1.33	1.68	27.0	3.80	2.85	1.33	1.46

In order to carry out a prediction of the flow in the S-shaped duct, it is important to ensure that the inlet boundary conditions match those occurring in the experiment. The measurements have fully defined the mean velocity and Reynolds stress profiles at the first traverse plane, but not the dissipation rate of turbulent kinetic energy (ε). To define this a series of calculations for a straight annular duct were conducted starting with uniform values for the inlet velocity, turbulence energy (or its components in stress closure prediction) and ε. The guessed values for inlet turbulence and ε were adjusted until at some downstream station the predicted mean and turbulence profiles agreed as closely as possible with those measured. These profiles were then used as the inlet boundary conditions to the S-shaped duct predictions.

RESULTS AND DISCUSSION

Experimental Results

The mean flow field has been described previously by Britchford et al. (1993) from data obtained with a five hole pressure probe and is in good agreement with the LDA measurements presented here. It should also be noted these measurements provide a large amount of information on the turbulent flow field. However, in this paper only the streamwise velocity (U) and main shear stress component ($\overline{uv}$) are presented in order to describe the main flow features. A summary of the boundary layer properties derived from the measured mean velocity profiles is given in Table 1. Note that the wall friction coefficient (C_f) has been calculated as $(U_\tau/U_{mean})^2$ so that direct comparison with the shear stress plots is possible.

Inlet Conditions. At inlet to the S-shaped duct the turbulent boundary layers that have developed along the inner and outer casings within the entry section each occupy approximately 24% of the passage height. In contrast, within the central portion of the passage a region of potential flow exists with a velocity of 30.3 m/s and an isotropic turbulence level of 0.17 m/s. The

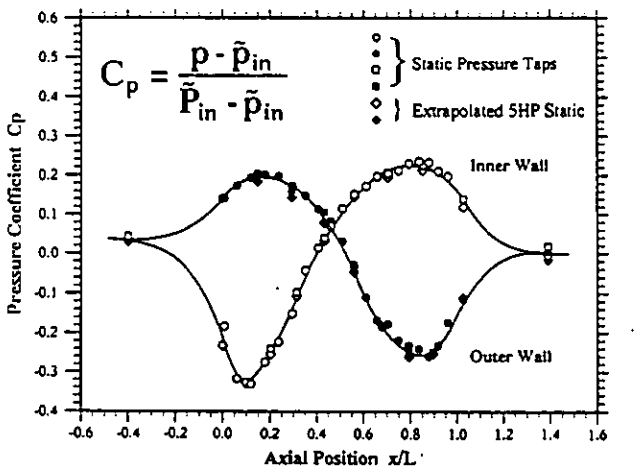

FIGURE 2 AXIAL VARIATION OF STATIC PRESSURE COEFFICIENT

spatial average velocity for the annular passage (U_{mean}) is 28.3 m/s with the radial and circumferential components of velocity being approximately zero. A more complete description of the inlet conditions is given by Carrotte et al. (1993). Note that U_{mean} at inlet has been used as a reference velocity to non-dimensionalise the mean velocity and shear stress data at all locations.

Static Pressure and Curvature Distribution. The development of each boundary layer is significantly affected by the static pressure distribution within the S-shaped duct (Fig. 2). Note that this distribution is expressed in terms of a static pressure coefficient (Cp) which is defined using the mass weighted total and static pressures at inlet to the duct (x/L=0.0). For a given axial location, differences between the static pressure on each wall reflect how the pressure field adjusts in order to provide the required radial forces to turn the flow. Thus, within the first bend pressures are relatively high and low for the outer and inner casings respectively, but this situation is reversed as the flow is returned to the axial direction within the second bend. As a result significant streamwise pressure gradients occur, with the inner wall boundary layer being subjected to a predominantly positive (i.e. adverse) gradient as the static pressure coefficient rises from –0.33 to +0.22 along approximately 70% of the duct length. In contrast, the pressure gradient is mostly negative (i.e. favourable) for the outer wall boundary layer with the coefficient reducing from +0.20 to –0.26 along a similar length.

In addition to streamwise pressure gradients, the development of each boundary layer is also influenced by the curvature effects which modify the flow's turbulence structure. The relative magnitude of these effects is indicated by the non-dimensional streamwise pressure gradient parameter, $(\delta^*/\tau_w).(\partial p/\partial x)$, and the curvature parameter $\delta.K_{eff}$ ($\equiv\delta/R$). These have been

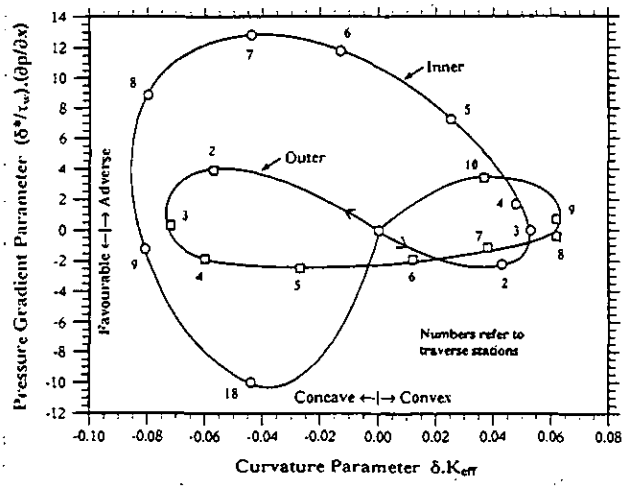

FIGURE 3 VARIATION OF NON-DIMENSIONAL CURVATURE AND PRESSURE GRADIENT

calculated for each traverse plane and are presented graphically (Fig. 3). Along the inner wall, these parameters indicate the flow is initially subjected to a modest favourable pressure gradient as the convex (stabilising) curvature increases up to a maximum value. Downstream of this location the flow is then subjected to a sustained region of increasing pressure, between approximately 12% to 80% of the duct length, with the adverse gradient reaching a maximum value at the 60% location. During this time the curvature has gone from being convex to concave, the maximum concave value occurring approximately 80% along the duct. Finally, in the latter stages of the duct the inner wall flow is subjected to a strong favourable pressure gradient with the concave curvature decreasing towards the duct exit. For the outer wall boundary layer it is apparent that, despite the absolute pressure gradients being comparable with those along the inner casing (Fig. 2), the non-dimensional static pressure gradients are smaller. This denotes that the relative effect on the boundary layer, due to streamwise pressure variations, is reduced because of the small displacement thickness and high values of wall shear stress. It can be seen that along the outer wall the pressure gradient is adverse within the initial and latter stages of the duct, with a modest favourable gradient between the 12% and 80% locations. At the same time the flow, for 45% of the duct length, is subjected to concave curvature which is then followed by convex curvature of comparable magnitude.

It should be noted that the magnitude of the curvature parameter suggests the flow within the duct is experiencing strong curvature, similar to that described by Gillis and Johnston (1983) and Barlow and Johnston (1983). This, combined with the continually varying pressure gradients, gives rise to the development of a complex flow along each casing.

Turbulent Shear Stress Distribution. The measured distribution of shear stress ($\overline{uv}$) along the length of the duct is shown in Fig. 4. For reasons of brevity this is the only component of Reynolds stress presented, the full set of turbulence data being given by Britchford (1994). Natural development of the boundary layers in the entry length (up to x/L=—0.4) produces the normal linear distribution of shear stress, which when extrapolated to the wall is in good agreement with the value of C_f derived from the mean velocity data.

Along the inner wall, the flow reacts quickly to the onset of strong convex curvature leading to a suppression of the shear stress in the outer part of the boundary layer. In the experiments of Gillis and Johnston (1983) a distance of one or two boundary layer thicknesses was required for such effects to be observed. At the same time an initially favourable pressure gradient leads to an increase in the near wall momentum and a high wall shear stress. However, by station 5 (x/L=0.375) the pressure gradient has altered to that of adverse (decelerating) resulting in a reduction of the near wall momentum; whilst at the same time the shear stress in the outer part of the layer remains suppressed. As the boundary layer continues to grow so the wall shear stress decreases and the peak value moves progressively further from the wall, whilst satisfying the condition $(\partial\tau/\partial y)_{y=0} = (\partial p/\partial x)$. Although by station 6 (x/L=0.50) the curvature of the inner wall has changed to concave the shear stress in the outer layer is still quite low and not until station 8 (x/L=0.75) does the effect of concave curvature lead to an increase in the outer layer shear stress. At the exit station where the pressure gradient is favourable and curvature is very small, the wall shear stress increases. However, the inherent lag of the turbulence structure, relative to the mean velocity, results in a very similar shear stress distribution to that observed at station 8 which is equivalent to a distance of 2 boundary layer thicknesses upstream of the exit plane.

Along the outer wall concave curvature increases the shear stress in the outer part of the boundary layer whereas the adverse pressure gradient reduces the near wall momentum and wall friction. However as the pressure gradient changes to that of favourable (accelerating) so the wall shear increases but curvature ensures that a high level of mixing persists in the outer layer. Not until station 8 (x/L=0.75) does the influence of convex curvature lead to a significant reduction in outer layer shear. In the latter part of the duct, there is insufficient distance for the effect of the comparatively small non-dimensional pressure gradient to have an observable effect on the shear stress distribution at x/L=1.0.

Mean Velocity Profile. At a given location the mean fluid velocity is a function of the applied streamwise pressure gradient and the turbulent shear stress. In this way the duct curvature directly affects the velocity profile, through the static pressure field, and indirectly through the modified turbulence structure. The mean velocity profiles show the presence of a potential core region, along the entire length of the duct, which isolates the boundary layers adjacent to each casing (Fig. 5). The development of these boundary layers is indicated in greater detail by the integral parameters contained in Table 1. Of

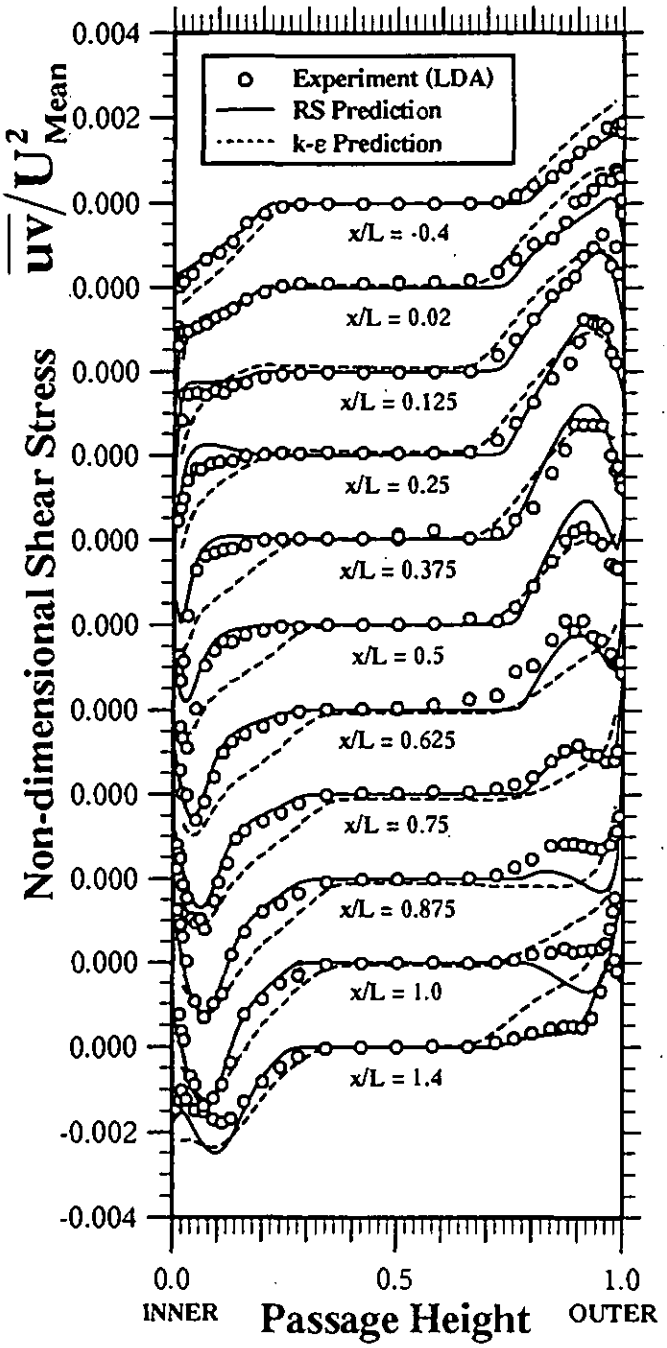

FIGURE 4 COMPARISON OF MEASURED AND PREDICTED SHEAR STRESS PROFILES

particular significance is the variation of each boundary layer's shape parameter (H) along the duct which shows that it is the flow adjacent to the inner casing that is most likely to separate (Fig. 6). This is due to the combined influence of the sustained adverse pressure gradient and the outer layer's suppressed shear stress associated with earlier convex curvature. This gives rise to the rapid growth in shape parameter which reaches a maximum value of 1.66 at x/L=0.75. However, it should be noted that this is well below the value of approximately 2.4 associated with flow nearing separation. Downstream of this location the favourable pressure gradient and increased mixing due to concave curvature leads to a rapid reduction of the shape parameter. Although no struts were included it is interesting to speculate on the way in which they may influence development of the flow. Normally struts are located over a substantial proportion of the duct length and have an aerofoil cross section. Clearly there is a need to avoid local flow separation in the region of adverse pressure gradient that normally occurs downstream of the point of maximum thickness. However when immersed in the S-shaped duct the pressure distribution on the surface of the strut will be a function of the local velocity and pressure fields. Hence, near the centre and outer wall regions separation is unlikely whereas near the inner wall attention to the strut profile may be required if separation is to be prevented.

Comparison of Experimental and Theoretical Results

The predictions made with both k-ε and second moment closure models are compared against the measured Reynolds shear stress (Fig. 4) and mean velocity (Fig. 5) data. Britchford et al. (1993) have already discussed the performance of the two turbulence models with regard to predicting the mean velocity profiles, and so emphasis is placed here on the comparison with the measured shear stress data. The procedure for developing the profiles of shear stress at inlet to the S-shaped duct (i.e. at x/L=−0.4), as described in a previous section, is slightly more successful with the Reynolds stress model than the eddy viscosity closure. This is perhaps because $\overline{uv}$ is solved for independently, rather than being tied closely to the mean velocity profile. However, differences between the two models at stations further downstream are more associated with modelling assumptions, rather than slight discrepancies of inlet conditions.

The $\overline{uv}$ profiles on the inner wall at x/L=0.02 and 0.125 show that the Reynolds stress model is much more successful at capturing the different effects of streamwise pressure gradient and streamline curvature on different portions of the shear stress profile. In the immediate vicinity of the wall the very steep gradient of $\overline{uv}$ is a response to the effect of the pressure gradient on the mean velocity, whereas the shape and level of $\overline{uv}$ between 5% and 20% of the annulus height away from the wall describes the suppression of $\overline{uv}$ as a response to streamline curvature. The k-ε predictions, in contrast to the experimental data, show no clearly discernible two-layer shape to the profile. Unfortunately, the stress model seems to be too sensitive to curvature effects, because in the region of maximum convex curvature (between stations 3 and 4) the $\overline{uv}$ is predicted to change sign, whereas the data only approach zero. However, the adverse pressure gradient effect which produces a peak in the inner wall shear stress in the region x/L=0.375 onwards is well represented in the stress model prediction, whereas it only

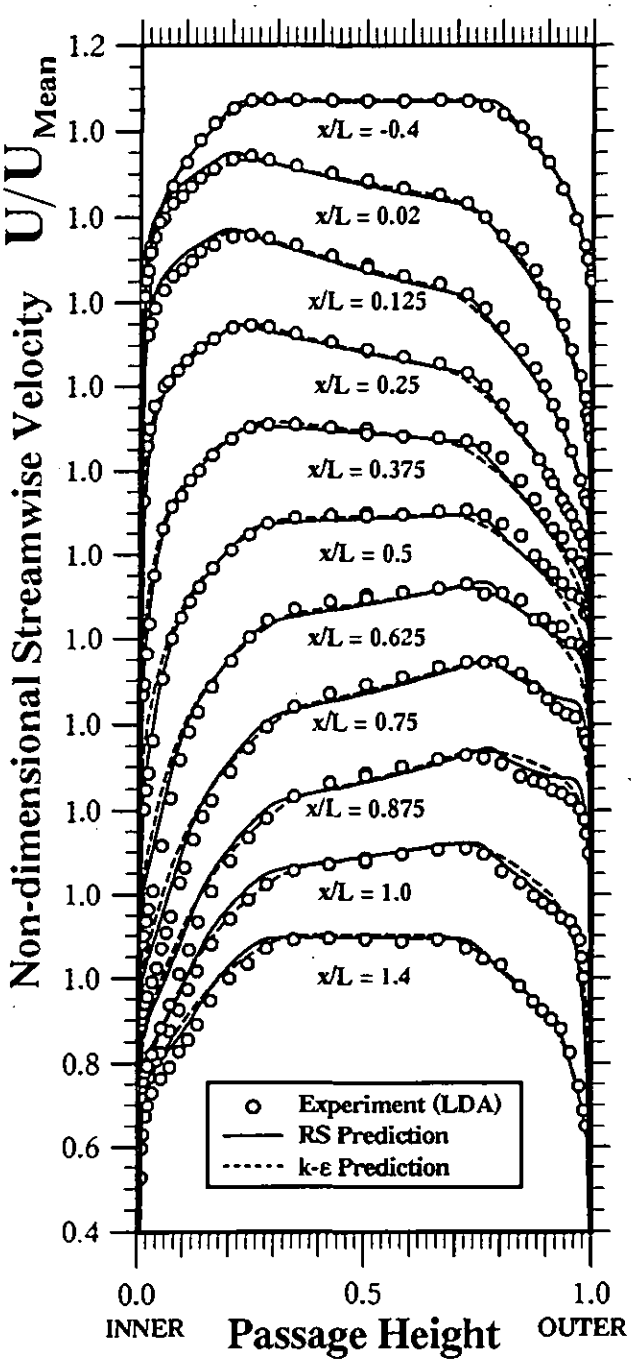

FIGURE 5 COMPARISON OF MEASURED AND PREDICTED STREAMWISE VELOCITY PROFILES

appears at x/L=0.625 in the k-ε prediction, and even then implies much too large a value for the wall shear stress.

On the outer wall, apart from the increasing stress level due to concave curvature which is captured by both models, the most noticeable differences occur downstream of station 8 when the combination of convex curvature and adverse pressure gradient begins. Both measurements and stress transport model predictions show a clear maximum/minimum shape which is not displayed at all by the eddy viscosity model: the clearest example of this may be seen in the profile at station 8. Once again, an over prediction of the curvature effect may be observed in the stress model (most noticeably at x/L=1.0).

As a consequence of the more accurate simulation of the shear stress profile, the mean velocity profile shapes are better predicted by the stress model, as reported by Britchford et al. (1993). From the design viewpoint, the most important consequence of this is that the error between the k-ε prediction and the measured shape parameter, at the location of maximum value (x/L=0.7 on the inner wall), is halved by moving to a stress transport closure (Fig. 6). The implication here is that if a duct design is likely to be close to separation, the critical case would be predicted much better by the stress transport model rather than an eddy viscosity scheme.

CONCLUSIONS

The LDA measurements indicate that the development of the flow within the duct is complex and significantly influenced by the combined effects of streamwise pressure gradient and flow curvature. Whereas curvature effects are not described properly by the k-ε calculation, such effects are captured more accurately by the Reynolds stress model leading to a better prediction of the Reynolds shear stress distribution. This, in turn, leads to a more accurate prediction of the mean velocity profiles, as reflected by the boundary layer shape parameter, particularly in critical regions of the duct where peak shape factors occur.

The tests reported form part of a programme aimed at obtaining a better understanding of the flow in S-shaped ducts and earlier work (Britchford et al., 1993) has already indicated that, with a compressor upstream, the peak value of shape parameter is reduced along the inner wall. Currently tests are in hand to measure the turbulence structure with the compressor at inlet and to investigate the influence of struts. Before CFD predictions can be used with confidence to improve duct designs the superiority of the stress closure over the k-ε model, as observed for the clean duct, must also be confirmed for the case with compressor inlet conditions and with a duct flow much closer to separation than observed here. These tests also form part of a continuing programme of work at Loughborough.

ACKNOWLEDGEMENTS

The authors would like to express their thanks to R. Marson, D. Glover, L. Monk and W. Niven for their help in the construction of the test facility, and to Dr. A. P. Manners and D. Bailey for their assistance in carrying out the CFD predictions. The work was sponsored by SERC and Rolls-Royce plc.

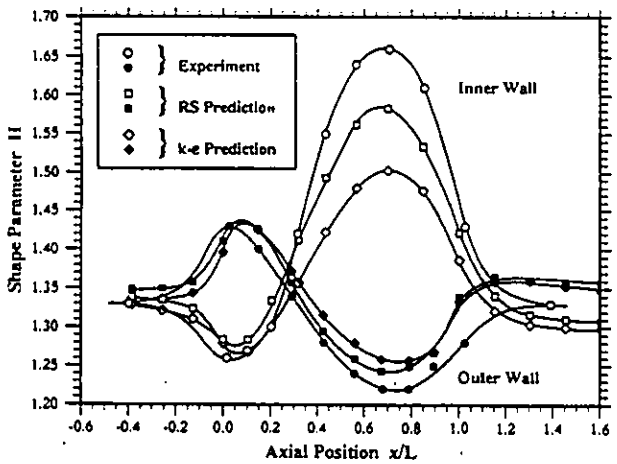

FIGURE 6 AXIAL VARIATION OF MEASURED AND PREDICTED SHAPE PARAMETER

REFERENCES

Bandyopadhyay, P. R. and Ahmed, A., 1993, "Turbulent Boundary Layers Subjected to Multiple Curvatures and Pressure Gradients", Journal of Fluid Mechanics, Vol. 246, pp. 503-527.

Barlow, R. S. and Johnston, J. P., 1988, "Structure of a Turbulent Boundary Layer on a Concave Surface", Journal of Fluid Mechanics, Vol. 191, pp. 137-176.

Baskaran, V., Smits, A. J. and Joubert, P.N., 1987, "A Turbulent Flow over a Curved Hill. Part 1. Growth of an Internal Boundary Layer", Journal of Fluid Mechanics, Vol. 182, pp. 47-83.

Bradshaw, P., 1973, "Effects of Streamline Curvature on Turbulent Flow", AGARD AG-169.

Britchford, K. M., Manners, A. P., McGuirk, J. J. and Stevens, S. J., 1993, "Measurements and Prediction of Flow in Annular S-shaped Ducts", Proceedings of the Second International Symposium on Engineering Turbulence Modelling and Measurements, Florence, Italy, pp. 785-794.

Britchford, K. M., 1994, "The Aerodynamic Behaviour of Annular S-shaped Ducts", Ph.D. Thesis (to be submitted), Department of Transport Technology, Loughborough University.

Carrotte, J. F., Britchford, K. M. and Wray, A. P., 1993, "Three Component LDA Measurements of Annulus Wall Boundary Layers Upstream of an Annular S-shaped Duct", Proceedings of the Fifth International Conference on Laser Anemometry Advances and Applications, Veldhoven, The Netherlands, pp. 111-118.

Gillis, J. C. and Johnston, J. P., 1983, "Turbulent Boundary Layer Flow and Structure on a Convex Wall and its Redevelopment on a Flat Wall", Journal of Fluid Mechanics, Vol. 135, pp. 123-153.

Hoffmann, P. H., Muck, K. C. and Bradshaw, P., 1985, "The Effect of Concave Surface Curvature on Turbulent Boundary Layers", Journal of Fluid Mechanics, Vol. 161, pp. 371-403.

Jones, W. P. and Manners, A. P., 1989, "The Calculation of the Flow Through a Two-dimensional Faired Diffuser", Proceedings of the Sixth Symposium on Turbulent Shear Flows, Toulouse, France, pp. 17.7.1-17.7.5.

Meroney, R. N. and Bradshaw, P., 1975, "Turbulent Boundary Layer Growth over a Longitudinally Curved Surface", AIAA Journal, Vol. 13, pp. 1448-1453.

Moser, R. D. and Moin, P., 1987, "The Effect of Curvature in Wall-bounded Turbulent Flows", Journal of Fluid Mechanics, Vol. 175, pp. 479-510.

Muck, K. C., Hoffmann, P. H. and Bradshaw, P., 1985, "The Effect of Convex Surface Curvature on Turbulent Boundary Layers", Journal of Fluid Mechanics, Vol. 161, pp. 347-369.

Schubauer, G. B. and Klebanoff, P. S., 1951, "Investigation of Separation of the Turbulent Boundary Layer", NACA Report No. 1030.

Shivaprasad, B. G. and Ramaprian, B. R., 1978, "Turbulence Measurements in Boundary Layers along Mildly Curved Surfaces", ASME Journal of Fluids Engineering, Vol. 100, pp. 37-46.

So, R. M. C. and Mellor, G. L., 1972, "An Experimental Investigation of Turbulent Boundary Layers along Curved Surfaces", NASA CR-1940.

Stevens, S. J. and Eccleston, B., 1969, "The Performance of Combustion Chamber Annular Diffusers", Department of Transport Technology Report No. TT69R02, Loughborough University.

Tsuji, Y. and Morikawa, Y., 1976, "Turbulent Boundary Layer with Pressure Gradient Alternating in Sign", Aeronautical Quarterly, Vol. 27, pp. 15-28.